Effect of Repeated Repair Metal Inert Gas Welding on Microstructural Properties, Corrosion Resistance, and Wear Behavior of 5083-H116 Aluminum Alloy

Mohammad Reza Zarghamian[1], Mansoor Farzam[2*], Iman Danaee[3], and Hadi Eskandari[4]

[1] M.S. Student, Department of Technical Inspection, Petroleum University of Technology, Abadan, Iran
[2] Associate Professor, Department of Technical Inspection, Petroleum University of Technology, Abadan, Iran
[3] Associate Professor, Department of Technical Inspection, Petroleum University of Technology, Abadan, Iran
[4] Assistant Professor, Department of Technical Inspection, Petroleum University of Technology, Abadan, Iran

Abstract

The effect of repeated repair welding, shielded with argon, on microstructural properties, corrosion resistance, and dry sliding wear behavior of aluminum alloy 5083/H116 were investigated. Samples were welded by metal inert gas welding method. 100% argon was used to protect fusion zone. Aluminum alloy 5356 was used as the filler metal. The samples for microstructure, corrosion, and wear tests were prepared from welded and repaired plates. To study the microstructural properties, the samples were mounted, polished, and then etched by the Keller's solution. Optical microscopy was used for metallurgical analysis. The corrosion behavior was evaluated in 3.5% NaCl solution and at a temperature of 25 °C using a potentiodynamic polarization and electrochemical impedance spectroscopy methods. Dry sliding wear behavior was evaluated by pin on disc method and scanning electron microscopy.

1. Introduction

Today, some industries are trying to produce not only quality parts but also lighter ones. Metals such as aluminum are in great use in this regard. Some ship hulls, structures, pressure vessels, and pipelines are made of aluminum alloys. Aluminum alloy 5083-H116 similar to other aluminum alloys in 5xxx series has a high strength, corrosion resistance, and high weldability. As a result, 5*xxx* aluminum alloys have found a wide application in building and construction; highway structures, (including bridges); storage tanks and pressure vessels in refineries and petrochemicals; cryogenic tankage and systems for temperatures as low as -270 °C (-455 °F) or near absolute zero; and marine applications. High-speed, single-hull ships employ 5083-H116/H321 machined plate for hulls, hull stiffeners, decking, and superstructure. Defects are created during producing and welding process, so repairing the welds is necessary. This kind of repair welding is used in oil and gas industry for engineering parts, vessels, piping etc. Most of the investigations about 5083 aluminum alloy studied the friction stir welding and processing of this alloy (Hirata et al., 2007; Borrego et al., 2014; Choi et al., 2013; Chen et al., 2008;

---

* Corresponding Author:
    Email: farzam@put.ac.ir

Gungor et al., 2014). It has been reported that the type of intermetallic particles in aluminum alloys plays a major role in passivity breakdown and pit morphology of aluminum alloys in seawater (Ezuber et al., 2008). The corrosion and mechanical properties of aluminum alloy 5083-H116 in metal inert gas welding based on slow strain rate test has also been investigated. According to investigation on the electrochemical experiments for the base metal and weld metal, the overall anodic polarization trend of the weld metal was good due to the formation of a passivation layer (Kim et al., 2010). The wear coefficient and reliability of sliding wear test procedure have been studied for high strength aluminum alloy and its composites. The study showed that wear coefficient decreased with increasing applied pressure and reached a minimum value; it then increased when the applied pressure reached near the seizure of the specimen. So far, very little research has been conducted on the effects of repair welding on mechanical and corrosion properties (Rao et al., 2010). In recent years, the effect of repair welding on microstructure, mechanical strength, and corrosion properties of 5083-H112 aluminum alloys welded with AA5183 filler wire in the presence of mixture of argon and helium as the shielding gas has been investigated. It was concluded that heating the parent metal (AA5083) close to the melting point resulted in grain growth phenomena and lead to the formation of continuous networks of precipitates at the grain boundaries; also, the overall corrosion behavior of the weldment was not significantly affected even in the extreme case of four repairs, since the more resistant regions tended to protect the more susceptible ones (Katsas et al., 2006; Katsas et al., 2007). An investigation into the repeated repair welding effect on the wear and corrosion properties of 5083-H116 aluminum alloy welded by ER5356 and shielded with argon has not been performed yet. To repair weld the samples, the upper passes of the weld were removed mechanically by a milling machine and re-welded in equal terms with the same filler metal under the same conditions. According to this method, instead of cutting and changing the damaged plate, one can repair it. This study evaluates the change in microstructure, wear behavior, and corrosion properties of 5083-H116 aluminum alloys after the repeated repair welding in NaCl 3.5% solution.
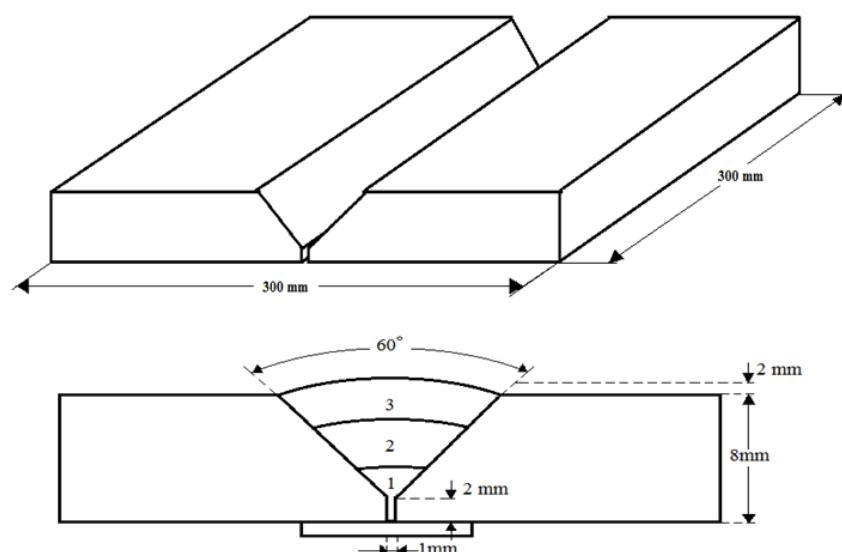
2. Experimental procedure

Aluminum alloy 5083-H116 was used as the base metal, which was welded with an AA5356 filler wire (Ø0.8 mm) (Liu et al., 1993). The chemical composition of the base and filler is shown in Table 1.

Table 1
Chemical composition (wt.%) of the parent metal AA-5083 and the filler wire AA-5356.

	Mn	Fe	Cu	Mg	Si	Zn	Cr	Ti	Al
5083	0.40-1.00	0.40	0.10	4.00-4.90	0.40	0.15	0.05-0.25	0.15	Balance
5356	0.05-0.20	0.40	0.10	4.50-5.50	0.25	0.10	0.05-0.20	0.06-0.20	Balance

Gas metal arc welding (GMAW) or metal inert gas (MIG) welding method was used. The shield gas was 100% argon (Liu et al., 1993). Preparing the baseplate was carried out according to Figure 1, and it was welded in a flat position (1G) (Liu et al., 1993).

Inter pass temperature measured with a digital multimeter was 50 °C. The polarity of welding was reversed (DCEP or DCRP) (Liu et al., 1993). Table 2 shows the details of the welding procedure and parameters (Liu et al., 1993).

Figure 1
Shape and dimensions of weldment specimens.

Table 2
Details and parameters of the welding procedure.

Welding method	Gas metal arc welding
Shielding gas	100% Argon
Gas flow	19 L/min
Diameter of nozzle opening	15 mm
Current type	Direct current reverse polarity (DCRP)
Base metal thickness	8 mm
Amperage	220-230 amps
Voltage	26 volts
Rate of wire feed	19 m/min

The samples were inspected using ultrasonic testing method (ASTM, V.03.03). To repair the weld, the upper passes of the weld were removed mechanically by a milling machine and re-welded in equal terms with the same filler metal under the same conditions. R0 is the sample that only welded once, and R1 is the sample repaired once, and so on. Repair welding was repeated up to 4 times (Katsas et al., 2006, and 2007; AghaAli et al., 2014). For metallurgical testing and analysis, the samples were cut, mounted, polished, and then etched. To polish the surface of the specimens, emery paper of grit Nos. 120, 400, 1200, 2500, and 3000 was used. Final polishing was with 0.25 μm Al_2O_3 suspensions, and the sample was then etched for 10-60 s in the Keller's solution (2 mL HF (48%), 3 mL HCl, 20 mL HNO_3, and 175 mL H_2O). Optical microscope (Model A. KRÜSS OPTRONIC) was used for metallurgical analysis (ASM, Vol. 9). The corrosion properties of the specimens were studied at room temperature. All specimens were mounted and the welded surface acted as the working electrode; the specimens immersed in 3.5% NaCl solution. The potentiodynamic polarization and impedance spectroscopy were conducted using AUTOLAB 302N instrument (ASTM, V.03.02). Autolab GPES software was used for evaluating the Tafel experimental data. Platinum and the silver/silver chloride (Ag/AgCl) were used as counter and referenced electrode respectively. Each specimen was scanned potentiodynamically at a scan rate of 1 mVs^{-1} from an initial potential of -1.0 V to a final potential of -

0.4 V (ASTM, V.03.02). The corrosion potential (E_{corr}) and corrosion current density (i_{corr}) were calculated from the intersection of the cathodic and anodic Tafel curves using the Tafel extrapolation method. The polarization resistance (R_P) is determined using Stern-Geary equation (ASTM, V.03.02):

$$R_P = \frac{\beta_a \beta_c}{2.303 i_{corr}} (\beta_a + \beta)_c \tag{1}$$

where, β_a (v/dec) is anodic Tafel slope, and β_c (v/dec) is cathodic Tafel slope.

Eelectrochemical impedance spectroscopy (EIS) measurements were performed in a frequency range between 100 kHz and 10 mHz. The peak-to-peak amplitude of the sinusoidal voltage signal was 10 mV. All EIS are recorded at the open circuit potential, and all the experiments were performed after an exposure period of 15-20 min until a steady state situation was recorded. The wear properties of the specimens were tested under dry conditions at room temperature (25 °C) using a wear test machine (ASTM, V.03.02, G-99). A schematic diagram of pin-on-disc apparatus is shown in Figure 2.
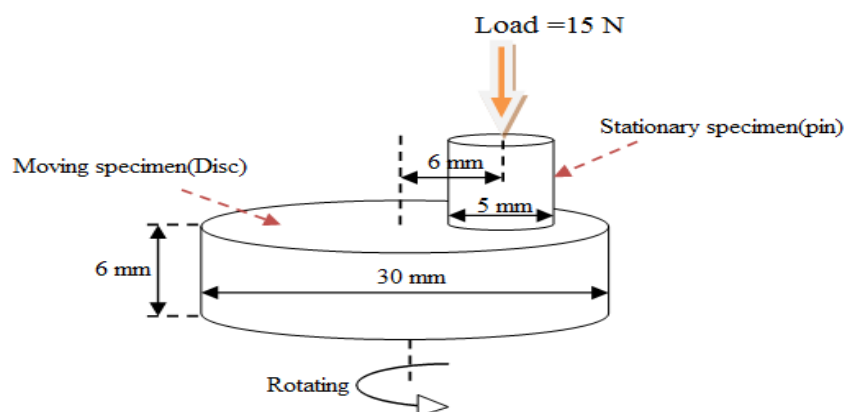

Figure 2
A schematic of the pin-on-disc wear test and the details of its parameters and dimensions of samples.

The pin is pressed against the disk (sample) at a load of 15 N by means of an arm or lever and attached weights. The machine caused the disk specimen to rotate, and the pin specimen was stationary; the rotating speed was 88 rpm. The accumulated sliding distance was 0.012 m, and the pin specimen was made of hardened AISI 52100 bearing steel with a HRC64, Ø hardness of, 5 mm and a surface roughness of $Ra = 0.06$ μm. The disk specimen diameter and thickness were 30 mm and 6 mm respectively. Before wear testing, the surface of the disk specimen was polished with emery paper (ASTM, V.03.02). The total sliding distance was 500 m increasing at an increment of 100 m. After each increment, the sample was removed; cleaned by acetone, dried, and weighted; and then remounted in the wear machine at the same location. The weight losses of discs were measured by an electronic balance having a sensitivity of ±0.1 mg. After wear testing, the surface of the specimens was analyzed by scanning electron microscopy (SEM, VEGA-TESCAN-XMU).

3. Results and discussion

3.1. Microstructural properties

The thickness of the base plate was 8 mm and the shielding gas was argon (100%). The examination of the microstructure focused the heat-affected zone. Argon has low thermal conductivity compared to the mixture of helium and argon; therefore, the grain size was fine (Peasura et al., 2012). Moreover, the grain size shows that the ß-phase intermetallic (Mg_5Al_8) precipitate is formed at the grain boundary (Mills et

al., 1985), so the distribution of ß-phase was further. By optical microscope, three regions, namely the weld zone, the heat-affected zone, and the base metal, were observed; the heat affected zone (HAZ) is between the other zones. The heat-affected zones of the samples (B.M, R0, R1… R4) were also compared with each other. As repair welding increased in number, the ß phase amount increased. Figure 3 shows the microstructure of 5083-H116 after welding and repair welding (image size 400x).
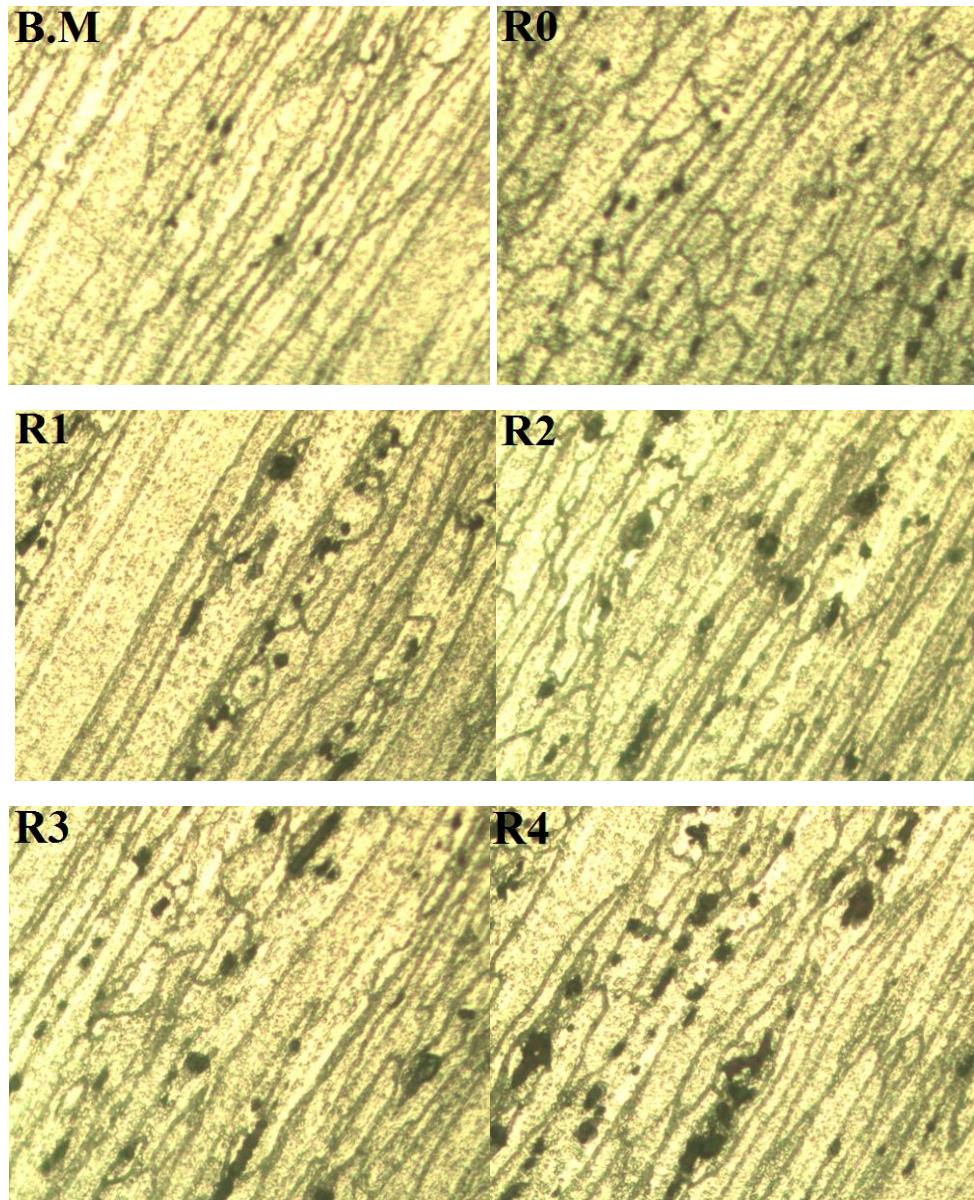

Figure 3
The microstructure of 5083-H116 after welding and repair welding, (image size 400x).

As can be seen in Figure 3, the distributions of ß-phase at the grain boundary in various repair welding specimens were further than R0, and they were also different from each other. The R0 specimen did not have any repair and was welded only once; thus, the distribution of ß-phase at its grain boundary was the least. Hence, by increasing the number of repairs, the distribution of ß-phase increased. During repair welding, the volume of materials removed and re-welded was not exactly equal, and the materials differed in the percentage of the elements in the repaired zone of the samples. Also, as a result of the repair technique, the weld-repaired samples were placed in additional thermal cycles which affected grain size

and microstructure evolution (Katsas et al., 2006, 2007). Furthermore, there is a large amount of porosities in the weldment of GMAW, especially in equiaxed crystal zone. Porosity is identified as the primary factor to deteriorate the mechanical properties of Al5083 weldment by GMAW (Ezuber et al., 2008). The difference in grain size, the presence of ß-phase, the presence of porosities, and the difference in the percentage of the elements in various samples will affect corrosion resistance, tensile, hardness, toughness, and wear properties of them (Liua et al., 2012).

3.2. Corrosion resistance in aerated NaCl

The Nyquist impedance diagram of the 5083/H116 series aluminum as-welded (R0) specimen in 3.5% NaCl solution at 25 °C is shown in Figure4.a, and the Nyquist diagrams of the 5083/H116 series aluminum weld-repaired specimens (R1-R4) are shown in Figure4.b.
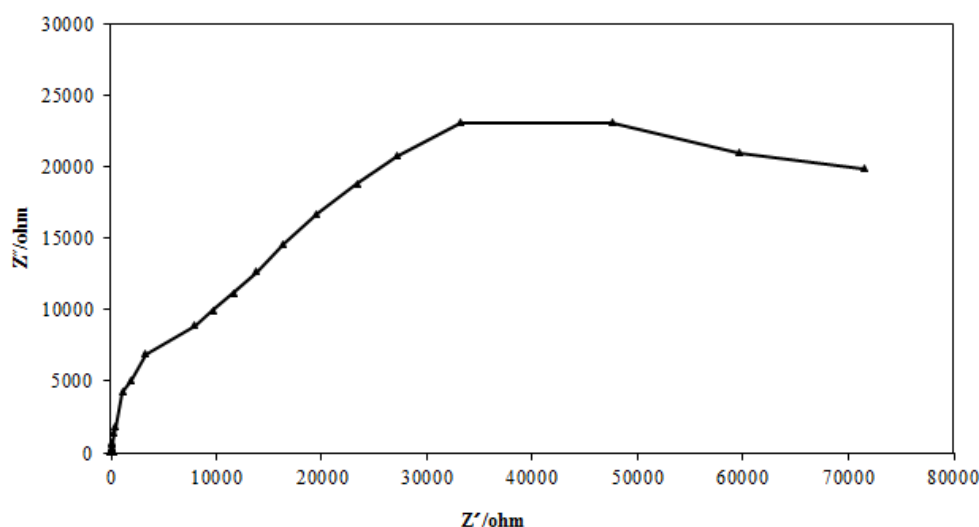

Figure 4.a
Nyquist impedance diagram of the 5083/H116 series aluminum as-welded (R0) specimen immersed in 3.5% NaCl solution at 25 °C.
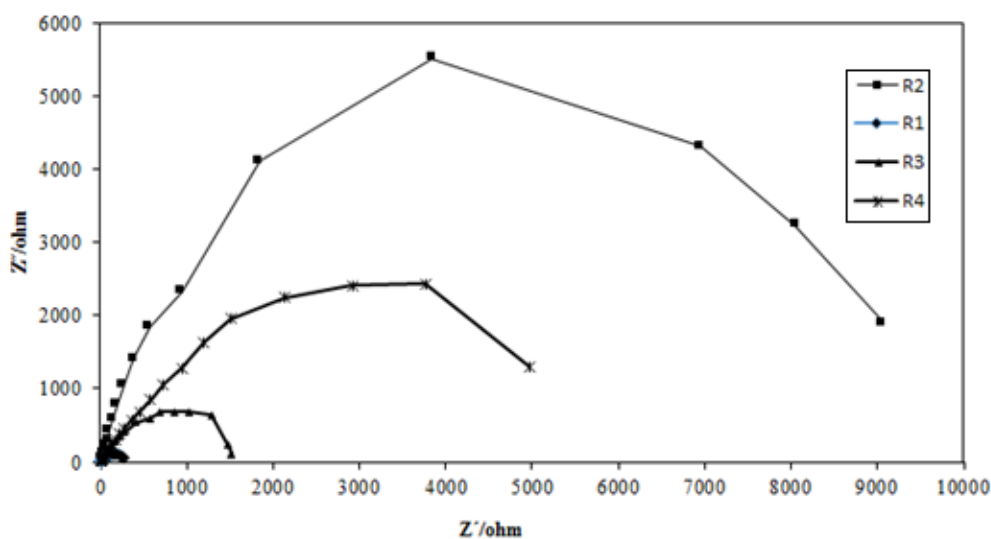

Figure 4.b
Nyquist impedance diagram of the 5083/H116 series aluminum weld-repaired R1, R2, R3, and R4 specimens immersed in 3.5% NaCl solution at 25 °C.

As can be seen, the corrosion rate of weld-repaired specimens is greater than that of the typical R0. Moreover, the corrosion rate of R1 is the greatest, while that of R2 is the smallest. The Tafel polarization curves are also shown in Figure 5.
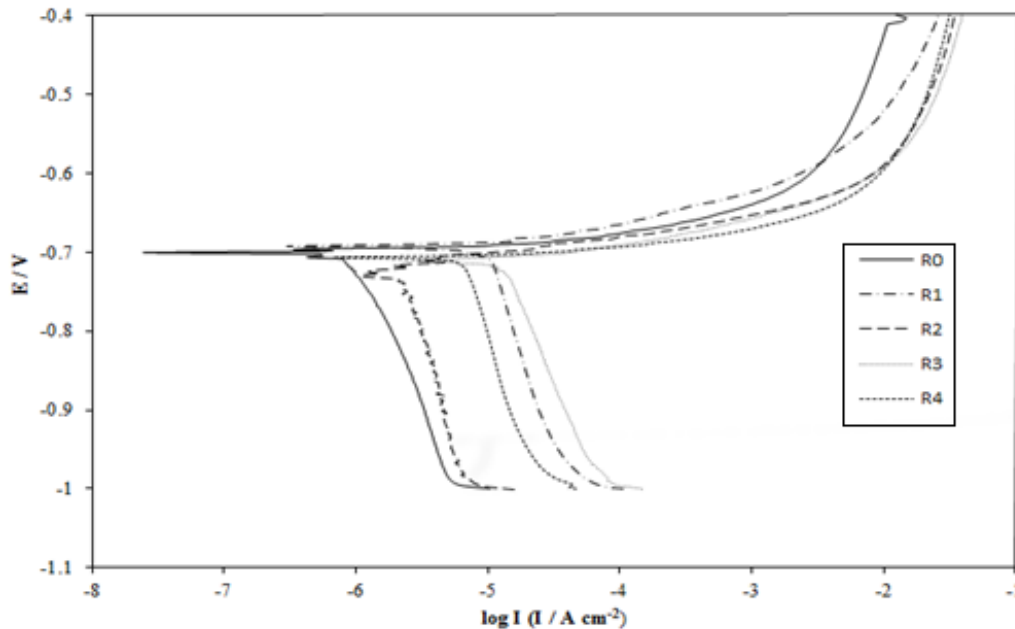

Figure 5

Tafel polarization curves of the 5083/H116 series aluminum for the as-welded and different weld-repaired specimens in 3.5% NaCl solution at 25 °C.

The measured data of the electrochemical parameters are presented in Table 3.

Table 3

Electrochemical properties of 5083/H116 series aluminum weld-repaired specimens immersed in 3.5% NaCl solution at 25 °C.

	β_c (v/dec)	β_a (v/dec)	I_{corr} (A/cm²)	E_{corr} (V)	Rp (ohm)	Corrosion rate (mm/year)
R0	0.015	0.076	2.925×10^{-7}	-0.703	$1.091 \times 10^{+3}$	3.435×10^{-3}
R1	0.028	0.060	2.738×10^{-6}	-0.695	$1.726 \times 10^{+2}$	3.216×10^{-2}
R2	0.028	0.383	1.305×10^{-6}	-0.727	$2.352 \times 10^{+3}$	1.533×10^{-2}
R3	0.022	0.202	6.69×10^{-6}	-0.711	$1.916 \times 10^{+2}$	7.857×10^{-2}
R4	0.019	0.115	2.852×10^{-6}	-0.710	$2.151 \times 10^{+2}$	3.350×10^{-2}

The R1 specimen has the maximum value of corrosion potential, while the R2 specimen has the minimum value of corrosion potential. The R3 specimen has the maximum value of corrosion current density, whereas the R0 specimen has the minimum value of corrosion current density. Thus, according to Table 3 and by comparing the Tafel polarization curves of the samples, it is obvious that the corrosion rates of R1 and R3 specimens are greater than those of the others. According to the microstructural properties, the grain sizes of various weld-repaired specimens were fine (Peasura et al., 2012), and the ß-phase was formed at the grain boundary (Mills et al., 1985). The intermetallic particles in aluminum alloys play a major role in the passivity breakdown and pit morphology of aluminum alloys in seawater (Ezuber et al., 2008). There was little difference in the corrosion rate of weld-repaired samples, which was ascribed to the difference in the volume of materials removed and re-welded and to the difference

in percentage of the elements in the repaired zone of the samples. Thus, the corrosion rate of R0 was less than that of the other samples. The corrosion resistance of AA5083 is associated with the presence of the *ß*-phase. As a result of the decided repair technique, the weld-repaired samples were in additional thermal cycles, which affected grain size and microstructure evolution (Rao et al., 2010); hence, the corrosion rate of R0 was the smallest.

3.3. Dry sliding wear

Weight loss of 5083/H116 series aluminum at each 100 m sliding pin-on-disc under different repair conditions at a velocity of 0.06 m/s and a vertical load of 15 N is tabulated in Table 4.

Table 4
Weight loss of disc (mgr.) at each 100m sliding pin-on-disc under different repair conditions; (Vertical force= 15N; Velocity= 0.06m/s).

	100 m	200 m	300 m	400 m	500 m
B.M	6.3	11.1	12.3	14.4	15.5
R0	10.5	13.2	15.7	18	19.6
R1	11.3	14.4	14.8	17.7	19.8
R2	8	10.5	11.4	13.7	15.9
R3	15.4	16.5	19.9	20.9	22.4
R4	12.1	14.2	16.7	20	20.6

The total sliding distance was 500 m (at an increment of 100 m. By comparing the weight loss of the samples during sliding, it is obvious that the R3 and R4 specimens show the highest weight loss. The R3 and R4 were in additional thermal cycles compared with the other samples, and the grain sizes of them were greater compared to the others (Peasura et al., 2012). Thus, the weight loss of R3 and R4 were the highest. Furthermore, it is obvious that base metal (B.M.) and R2 have lower weight losses. The weight loss of all the samples showed roughly the same slope, and the difference in the weight loss of all the samples was very low. Hence, by increasing the number of repairs, the weight loss increases. Figures 6a, 6b, and 6c display the friction coefficient of B.M., R3, and R4 specimens under the identical conditions.
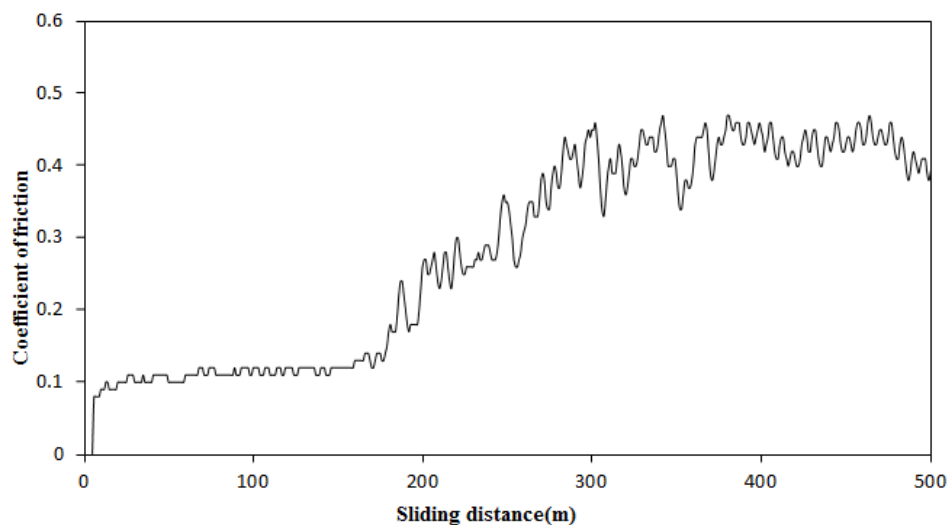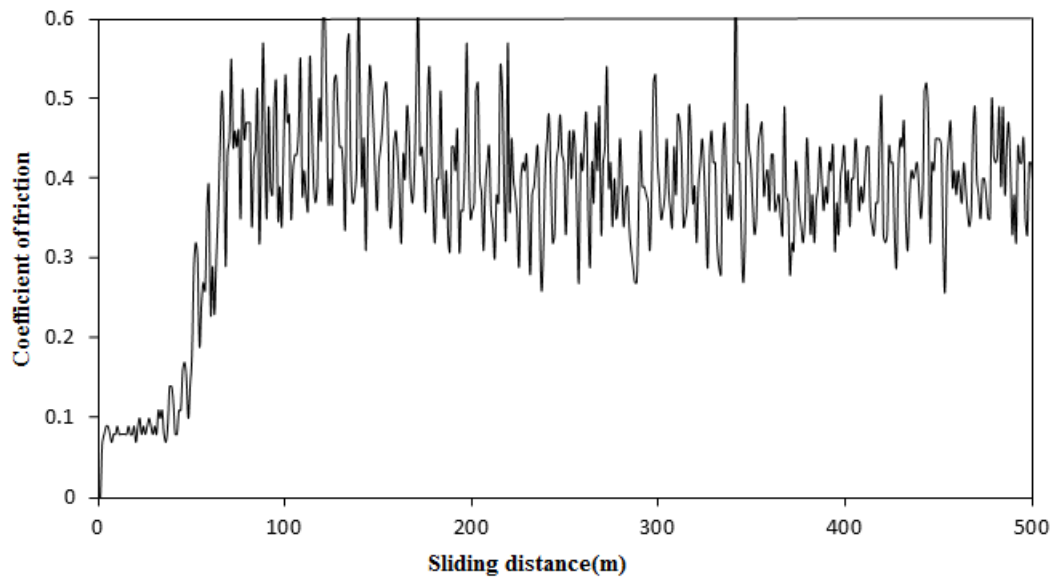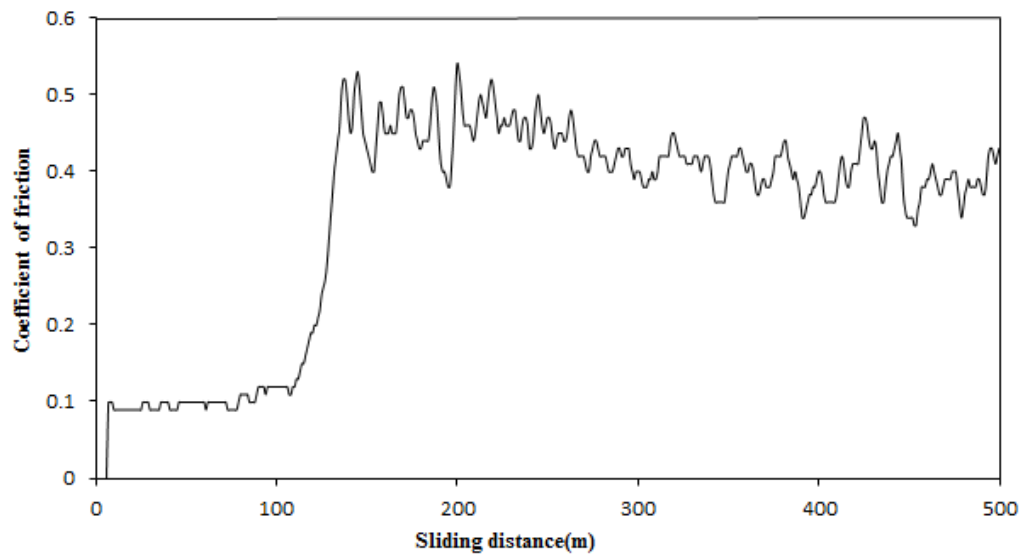

Figure 6.a
Friction coefficient curves of 5083-H116 aluminum alloy (base metal); (Vertical force= 15 N; Velocity= 0.06 m/s; Distance= 500 m).
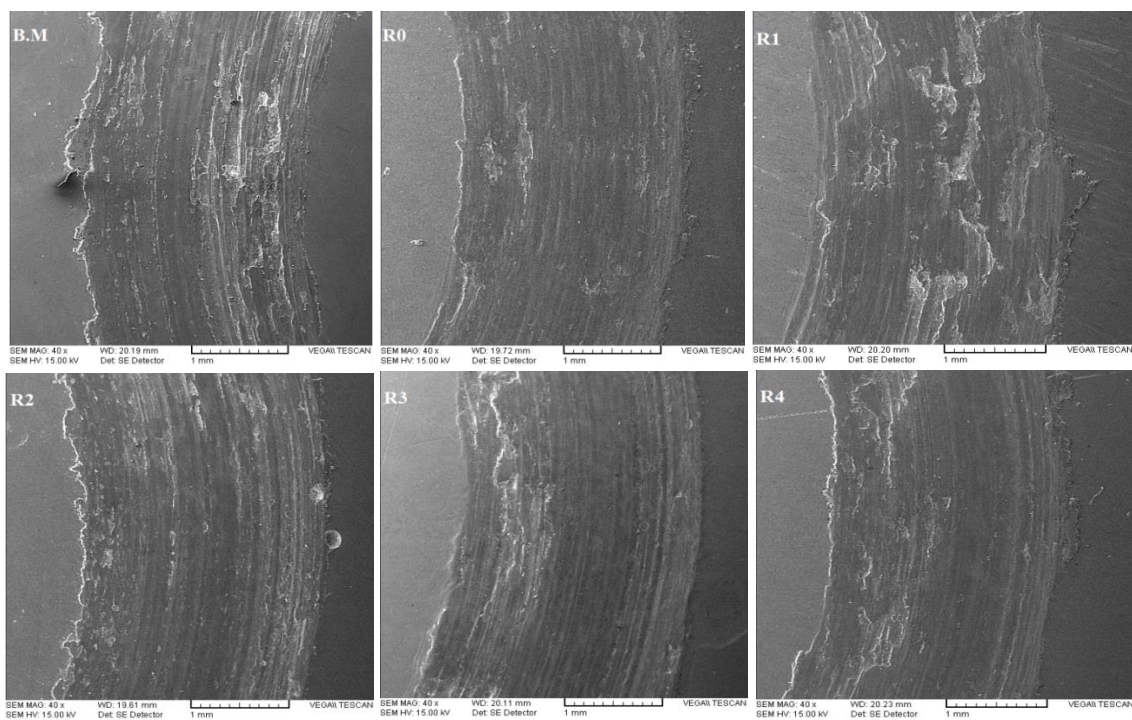
Figure 6.b
Friction coefficient curves of R3; (Vertical force= 15 N; Velocity= 0.06 m/s; Distance= 500 m).
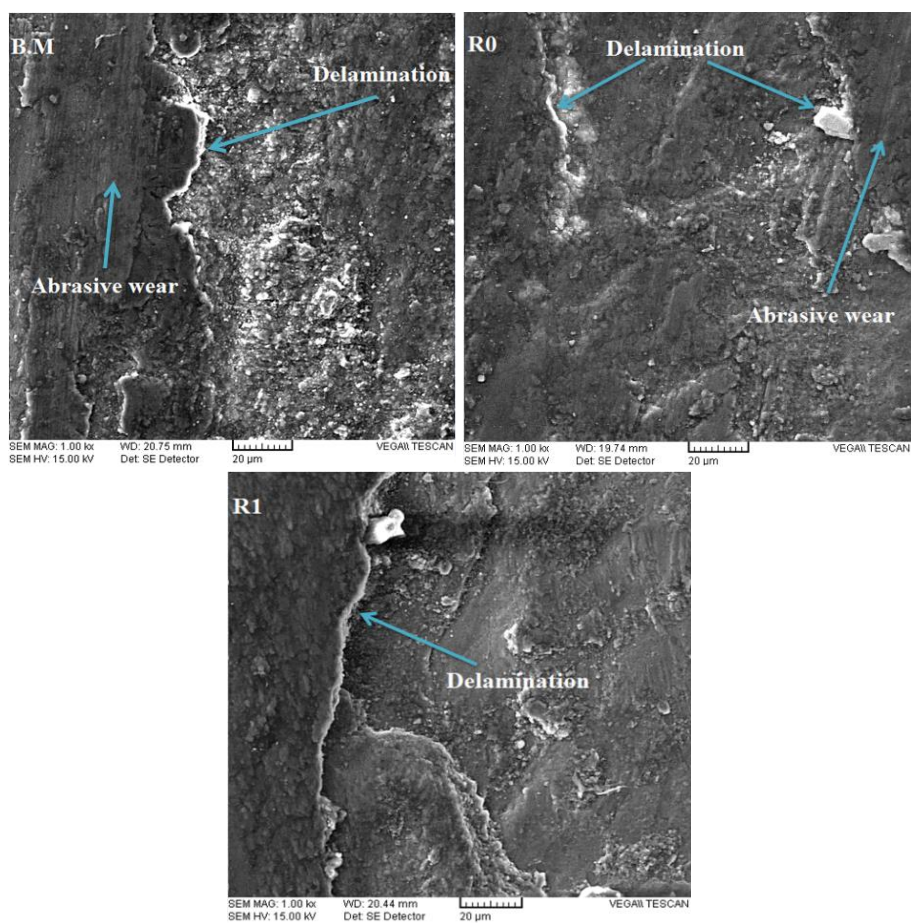

Figure 6.c
Friction coefficient curves of R4; (Vertical force= 15 N; Velocity= 0.06 m/s; Distance= 500 m).

The friction coefficients of all the specimens were the same at the first 50 m. By increasing the number of repairs, the ß-phase is formed at the grain boundary (Mills et al., 1985), so the distribution of ß-phase further results in an increase in the friction coefficient. According to the curves of friction coefficients, it is obvious that the friction coefficient of each repair sample rise to a maximum of 0.6; also, compared to the friction coefficient of the base metal specimen, the difference is very minimal. Figures 7 and 8 show the SEM micrographs of the wear surface of all the specimens.

Figure 7
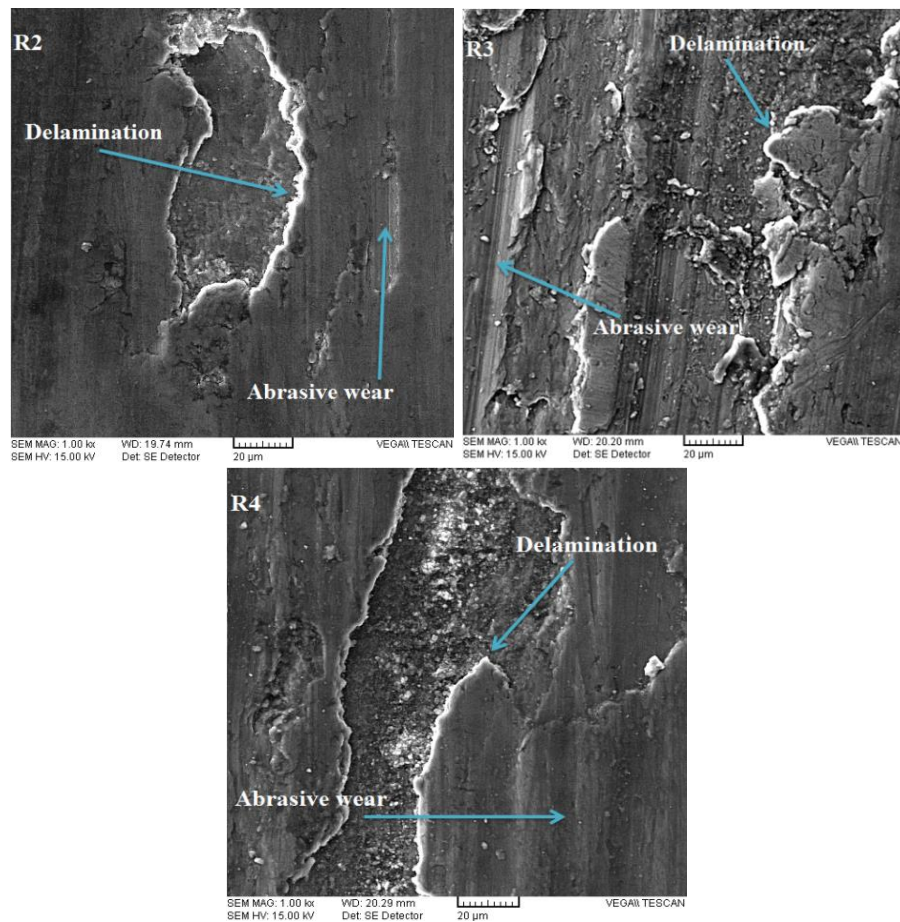The SEM of the wear surface of the specimens.

Figure 8
The SEM micrographs of the wear surface.

According to these figures, it is obvious that the kind of all the specimens is abrasive. Also, each SEM micrograph shows that the delamination phenomenon occurs. Since the difference in the grain size of the samples is very little (Katsas et al., 2006), the weight loss, the coefficient of friction, and the kind of wear in various samples are approximately similar.

4. Conclusions

In this study, the following conclusions can be drawn:

1. According to the results, the repeated repair welding does not influence the corrosion rate of 5083-H116 aluminum alloy.

2. Repeated repair welding, has no significant effect on the wear behavior of 5083-H116 aluminum alloy.

3. The mass loss of the 5083-H116 aluminum alloy after repeated repair welding in the same experimental conditions is approximately equal.

4. The increase in the coefficient of friction is between 0.5-0.6 in all the samples.

5. The kind of wear in all the experimental conditions is abrasive, and delamination occurs.

Nomenclature

AA	: Aluminum alloy
Al	: Aluminum
Amp	: Amperage
Ar	: Argon (Ar)
ASM	: American society for metals
ASTM	: American society for testing and materials
BM	: Base metal
Cr	: Chromium
Cu	: Copper
DCRP	: Direct current reverse polarity
E_{corr}	: Corrosion potential
EIS	: Electrochemical impedance spectroscopy
Fe	: Iron
GMAW	: Gas metal arc welding
HAZ	: Heat-affected zone
I_{corr}	: Corrosion current
MIG	: Metal inert gas
mL	: Milliliter
Mn	: Manganese
NaCl	: Sodium chloride
Ni	: Nickel
OM	: Optical microscope
R0	: Under no repair (as-welded)
R1	: One time repair
R2	: Two-time repair
R3	: Three-time repair
R4	: Four-time repair
R_P	: Polarization resistance
SEM	: Scanning electron microscopy
Si	: Silicon
β_a	: Anodic Tafel slope
β_c	: Cathodic Tafel slope
Ti	: Titanium
μm	: Micrometer

References

AghaAli, I., Farzam, M., Golozar, M. A., and Danaee, I., The Effect of Repeated Repair Welding on Mechanical and Corrosion Properties of Stainless Steel 316L, Materials and Design, Vol. 54, p. 331-341, 2014.

ASM Handbook, Vol. 9, Metallographic and Microstructure, USA, 1985.

ASM Handbook, Vol. 6, Welding, Brazing, and Soldering, 1993.

ASTM Standards. Vol. 03.02, Wear and Erosion, Vol. 03.03, Nondestructive Testing.

Borrego, L. P., Costa, J. D., Jesus, J. S., Loureiro, A. R., and Ferreira, J. M., Fatigue Life Improvement by Friction Stir Processing of 5083 Aluminum Alloy MIG Butt Welds, Theoretical and Applied Fracture Mechanics, Vol. 70, p. 68-74, 2014.

Chen, Z. W., Pasang, T., and Qi, Y., Shear Flow and Formation of Nugget Zone During Friction Stir Welding of Aluminum Alloy 5083-O, Materials Science and Engineering, Vol. 474, p. 312-316, 2008.

Choi, D. H., Ahn, B. W., Quesnel, D. J., and Jung, S. B., Behaviors of β Phase (Al_3Mg_2) in AA 5083 During Friction Stir Welding, Intermetallics, Vol. 35, p. 120-127, 2013.

Ezuber, H., El-Houd, A., and El-Shawesh, F., A Study on the Corrosion Behavior of Aluminum Alloys in Seawater, Materials and Design, Vol. 29, p. 801-805, 2008.

Gungor, B., Kaluc, E., Taban, E., and Sik, A., Mechanical, Fatigue and Microstructural Properties of Friction Stir Welded 5083-H111 and 6082-T651 Aluminum Alloys, Materials and Design, Vol. 56, p. 84-90, 2014.

Hirata, T., Oguri, T., Hagino, H., Tanaka, T., Chung, S. W., Takigawa, Y., and Higashi, K., Influence of Friction Stir Welding Parameters on Grain Size and Formability in 5083 Aluminum Alloy, Materials Science & Engineering, Vol. 456, p. 344-349, 2007.

Katsas, S., Nikolaou, J., and Papadimitriou, G., Corrosion Resistance of Repair Welded Naval Aluminum Alloys, Materials and Design, Vol. 28, p. 831-836, 2007.

Katsas, S., Nikolaou, J., and Papadimitriou, G., Microstructural Changes Accompanying Repair Welding in 5xxx Aluminum Alloys and Their Effect on the Mechanical Properties, Materials and Design, Vol. 27, p. 968-975, 2006.

Kim, S. J., Kim, S. K., and Park, J. C., The Corrosion and Mechanical Properties of Aluminum Alloy 5083-H116 in Metal Inert Gas Welding Based on Slow Strain Rate Test, Surface and Coatings Technology , Vol. 205, p. 573-578, 2010.

Liua, Y., Wangb, W., Xiea, J., Sunb, S., Wangc, L., Qiana, Y., Menga, Y., and Weia, Y., Microstructure and Mechanical Properties of Aluminum 5083 Weldments by Gas Tungsten Arc and Gas Metal Arc Welding, Materials Science and Engineering, Vol. 549, p. 7-13, 2012.

Peasura, P. and Watanapa, A., Influence of Shielding Gas on Aluminum Alloy 5083 in Gas Tungsten Arc Welding, Procedia Engineering, Vol. 29, p. 2465-2469, 2012.

Rao, R. N, and Das, S., Wear Coefficient and Reliability of Sliding Wear Test Procedure for High Strength Aluminum Alloy and Composite, Materials and Design, Vol. 31, p. 3227-3233, 2010.